

Josephson current through a quantum dot with spin-orbit coupling

L. Dell'Anna,¹ A. Zazunov,² R. Egger,¹ and T. Martin^{3,4}¹ Institut für Theoretische Physik, Heinrich-Heine-Universität, D-40225 Düsseldorf, Germany² LPMMC CNRS, 25 av. des Martyrs, F-38042 Grenoble, France³ Centre de Physique Théorique, Case 907 Luminy, F-13288 Marseille, France⁴ Université de la Méditerranée, F-13288 Marseille, France

(Dated: April 15, 2024)

The equilibrium Josephson current through a nanoscale multi-level quantum dot with Rashba or Dresselhaus spin-orbit coupling has been computed. The critical current can be drastically modified already by moderate . In the presence of a Zeeman field, Datta-Das-like oscillatory dependencies on are predicted.

PACS numbers: 74.78.Na, 74.50.+r, 71.70.Ej

I. INTRODUCTION

The Josephson effect provides a fundamental signature of phase coherent transport through mesoscopic samples with time reversal symmetry [1]. Here, we reconsider the theory of the Josephson effect through a quantum dot (QD) in a two-dimensional electron gas (2DEG), taking into account Rashba and/or Dresselhaus spin orbit (SO) couplings [2, 3]. Despite the large recent interest concerning SO effects in QDs, mainly caused by quantum information [4] and spintronics applications [5], the question of how the Josephson current is modified by SO couplings has barely been addressed. Naively, since SO couplings do not break time reversal symmetry, one may expect that they will not affect the Josephson effect at all. This expectation seems basically confirmed by the existing theoretical studies: In Ref. [6], the Josephson current through a perfectly contacted 2DEG with Rashba coupling is predicted to only show SO-related modifications in the simultaneous presence of a Zeeman field. In Ref. [7], the same conclusion has been reached for a single-channel conductor with arbitrary contact resistance. Moreover, in Ref. [8], by a generalization of earlier scattering approaches [9, 10], the case of a wide 2DEG with arbitrary contact resistance was studied, where the semiclassically averaged Josephson current is again found to be insensitive to Rashba SO couplings. However, the presence of a Josephson current through the mesoscopic system necessarily breaks time reversal invariance and therefore we reexamine this expectation in the present paper.

As 2DEG devices based on InAs-related materials are known to exhibit strong gate-tunable [11] Rashba SO couplings, and possibly Dresselhaus SO couplings, we study this problem here from the perspective of multi-level QD physics. Supercurrents through related devices have been probed by several experiments; for recent work, see Refs. [12, 13, 14, 15, 16]. It is thus not only of academic interest to quantitatively examine the effects of Rashba/Dresselhaus SO couplings on the equilibrium Josephson current. Moreover, very recently, gate-tunable supercurrents through thin InAs nanowires have been reported [17, 18], revealing complex current-phase relations such as π -junction behavior. Although we study a 2DEG geometry, our results are also relevant for such nanowires: the transport channels reside in a surface charge layer, and Rashba terms due to narrow-gap and strong confinement fields dominate over all other SO couplings. In those experiments, Josephson currents through few-level dots have already been achieved.

In the present work, we arrive at the surprising conclusion that SO couplings have huge effects on the Josephson current in nanoscale multi-level dots. Depending on the parameter regime, the critical current can be largely suppressed or enhanced. In a single-level dot, SO effects on the Josephson current vanish unless there is also a Zeeman field, but in multi-level dots no such restriction applies. The predicted strong dependence on SO couplings should be observable in state-of-the-art experiments. We also show that oscillations in the critical current I_c as a function of the distance L between the lead contacts appear under suitable conditions, resembling Datta-Das [5] spin precession effects.

The structure of the remainder of this paper is as follows. In Sec. II, the model is described. The Josephson current is calculated in Sec. III, and results are presented in Sec. IV for the simplest cases of one and two spin-degenerate levels. We conclude in Sec. V. Some details concerning the derivation of the Josephson current have been delegated to an Appendix.

where the transformed a_y is encoded in

$$A_{nn^0} = \frac{i}{m} \int_0^Z dr_n(r) [a_{y,n^0}(r)] e^{i \int_0^r dr_n(r') \cos[1 - 2\cos(2r') \sin^2(x)]} \frac{1}{\cos(2r) \sin(2x)} A; \quad (10)$$

and the Zeeman field leads to

$$B_{nn^0} \sim \int_0^Z dr_n(r) b e^{i g a_x} \sim e^{i g a_x} b_{nn^0}(r); \quad (11)$$

Since the dot electron wave function $\psi_n(r)$ in Eq. (7) can always be chosen real-valued, the $A_{i;nn^0}$ ($B_{i;nn^0}$) with $i = x, y, z$ represent antisymmetric (symmetric) Hermitian matrices in the QD levelspace. Finally, the transformation (8) yields the 2×2 spin matrices

$$U_{L=R} = \begin{pmatrix} \cos(L/2) & \sin(L/2)e^i \\ \sin(L/2)e^i & \cos(L/2) \end{pmatrix} \quad (12)$$

entering H_T in Eq. (6). The oscillatory dependence on the length L between the tunnel contacts appearing for $\phi \neq 0$ is due to a spin precession phase [5].

III. JOSEPHSON CURRENT

The equilibrium Josephson current at temperature T follows from the free energy $-T \ln Z$ via

$$I(\phi) = \frac{2e}{\hbar} T \partial_\phi \ln Z(\phi); \quad (13)$$

where the superconducting phase difference enters the BCS Hamiltonian (5). We adopt a functional-integral representation of the partition function Z , which here requires a slightly non-standard formulation due to the spin- $\frac{1}{2}$ terms. Given the fact that the Hamiltonian is quadratic in the fermion operators, the calculation should proceed in a straightforward manner. In the absence of spin- $\frac{1}{2}$ terms, such quadratic Hamiltonians are typically dealt with by introducing Nambu spinors. For the present case (see Appendix), the presence of spin- $\frac{1}{2}$ processes makes it necessary to introduce two types of Nambu spinors to describe the dot. In the end, the effective action describing the quantum dot coupled to the leads can nevertheless be written in terms of Grassmann fields $d_n(\tau)$ and $\bar{d}_n(\tau)$ for the dot fermions (τ is imaginary time). For a multilevel dot, we thus form the Nambu spinor for dot level n ,

$$\begin{pmatrix} d_n(\tau) \\ \bar{d}_n(\tau) \end{pmatrix} = \frac{1}{T} \sum_l e^{i l \tau} D_n(l); \quad (14)$$

with fermionic Matsubara frequencies $l = (2l+1)/T$ (integer l). Similarly, we define the Nambu multispinor

$$D(l) = (D_1(l); D_2(l); \dots)^T; \quad (15)$$

and then integrate out the lead fermions. As a result of this operation, $Z = \int D(D) e^S$ with the action

$$S = T \sum_{l>0} D(l); D(-l) \hat{S}_l \begin{pmatrix} D(l) \\ D(-l) \end{pmatrix}; \quad (16)$$

The apparent doubling of spinor space reflects our above discussion. This doubling does not create a double-counting problem, since only positive Matsubara frequencies l appear in Eq. (16). After straightforward but lengthy algebra, with $A_{i;nn^0} = A_{x;nn^0} - iA_{y;nn^0}$ (and likewise for B), see Eqs. (10) and (11), we find

$$\hat{S}_l = \begin{pmatrix} G_l^{-1} + A_z & A_x + iB_y \\ A_x - iB_y & G_l^{-1} + A_z \end{pmatrix} B_z; \quad (17)$$

The 2×2 structure refers to this doubled space, where each of the four entries represents a matrix in multispinor Nambu space, i.e. the Pauli matrices in Eq. (17) act in the Nambu (spin) sector, while A and B operate on the level space. Spin- $\frac{1}{2}$ transitions caused by SO processes are described by the off-diagonal entries A_x and B_y . Finally,

G_1 denotes the QD Green's function after integration over the leads but in the absence of SO couplings. This Green's function is derived and specified in the Appendix using the wide-band approximation, see Eq. (A 2), with the leads characterized by a constant normal-state density of states (assumed identical in both banks), and with the hybridization matrix

$$t_{L=R, mn^0} = \sqrt{t_{L=R, mn^0}} e^{i\phi_{L=R, mn^0}} \quad (18)$$

Note that eventually the $U_{L=R}$ factors do not contribute to the action, see Eq. (17), and thus the precession phase ϕ_L can appear only via A and B . We finally obtain from Eq. (13) the equilibrium Josephson current-phase relation,

$$I(\phi) = \frac{2e}{\hbar} T \sum_{n^0} \text{Im} \left[\frac{1}{\det \hat{S}_1} \right] \quad (19)$$

We stress that this result (given the model) is exact and does not involve approximations. The calculation of the Josephson current requires only a simple numerical routine and allows for a quantitative comparison to experimental data.

IV. APPLICATIONS

In order to get insight into the relevant physics, we here analyze the simplest cases of a single and of two spin-degenerate QD levels with symmetric hybridization matrix, $t_{L, mn^0} = t_{R, mn^0}$, $n^0=2$. While our conclusions are general, some coefficients below are model-dependent. They are derived for $V(r)$ given as hard-box confinement along the x-axis, $L=2 \times L=2$, plus a harmonic transverse confinement of frequency scale ω . The level index $n = (n_x, n_y)$ then contains the respective integer quantum numbers $n_x \geq 1$ and $n_y \geq 0$, with eigenenergy (up to an additive constant related to a gate voltage)

$$\epsilon_n = \frac{(\pi n_x L)^2}{2m} + \hbar \omega (n_y + 1/2) \quad (20)$$

in Eq. (7). Note that Eq. (19) contains not only the contributions of Andreev bound states but represents the full Josephson current. The necessity of computing the full current for finite L has been stressed recently [21].

A. Single dot level

Let us first address a single QD level, where we reproduce and extend previous results [6, 7]. The antisymmetry of A_{nn^0} implies $A = 0$, and thus SO couplings do not affect the Josephson current in the absence of a Zeeman field [6]. With $B = \beta$ given by

$$B^2 = (\hbar k_x \sin \phi - \hbar k_y \cos \phi)^2 + F_{n_x} \hbar^2 + (\hbar k_x \cos \phi + \hbar k_y \sin \phi)^2; \quad (21)$$

where F_n is defined as

$$F_n(L) = \frac{\sin^2(\pi n L)}{L(1 - \cos^2(\pi n L))}; \quad (22)$$

the determinant entering Eq. (19) is

$$\det \hat{S}_1 = 4 \left(\frac{\hbar^2}{2m} B^2 + \epsilon_n + \frac{\hbar^2}{2} + \frac{\hbar^2 \cos^2(\phi/2)}{\hbar^2 + \epsilon_n} \right) B^2; \quad (23)$$

where $\epsilon_n = \epsilon_n(1 + \frac{\hbar^2}{2m} \frac{1}{\epsilon_n^2 + \epsilon_n})$. Here we consider a situation where transport proceeds through a single resonant level with longitudinal quantum number $n_x \geq 1$, i.e. $\epsilon_{n_x} \approx 2m$ is close to zero, while the dot stays in the transverse ground state $n_y = 0$. Under the condition $\hbar \omega \gg \epsilon_n$ for the level spacing ϵ_n , i.e. for a quasi-1D situation, all states besides the n_x state close to resonance can be neglected, and one effectively has a single-level dot. Clearly, SO effects now can only enter via the effective magnetic field (21). Compared to the Andreev level spectrum of the $\mu = b = 0$ QD connected to superconducting electrodes, the combination of SO and Zeeman couplings gives rise to a splitting of the Andreev levels, giving in total four distinct levels. Each level carries a definite spin with

both spin up/down levels above/below the chemical potential. Superficially, the structure of this Andreev spectrum is somewhat analogous to the one of Ref. [22]. However, it is actually different because in Ref. [22] the levels refer to zero spin, spin up, spin down, and a spin singlet state, respectively. With Eq. (23) the Josephson current appears in precisely the form of the mean-field solution of the interacting Anderson dot problem obtained by Vecino et al. [23]. This implies that their results can be taken over (with their exchange energy E_{ex} being our B). In particular, the phase diagram in the B - ϕ plane exhibits rich behavior with four different phases including π -junction behavior, see Fig. 3 of Ref. [23]. In Fig. 1, the Josephson current is plotted as function of the phase difference. For simplicity, we consider $\phi = 0$ and gradually increase the effective magnetic field B given in Eq. (21). The transition to a π -junction with negative critical current occurs when $B > \frac{B_0}{2 + \sqrt{2}}$.

For $b_x = b_y = 0$, the oscillatory behavior of B due to the dependence of F_n on the spin precession phase L is most pronounced, with $B = 0$ for $L = 2\pi l$ (integer l). This oscillation may then persist in the Josephson current, suggesting the appearance of Datta-Das like oscillations in the critical current. These oscillations are displayed in Fig. 2; for $n_x = 1$, such oscillations are not yet observable, but they become visible for $n_x > 1$. Note that for convenience, the plots in Fig. 2 ignore the $\pi/2 = (2m)$ shift of n_x , as is appropriate for small ϕ ; alternatively, one could adjust a gate voltage on the quantum dot in order to bring the level into resonance. For $\phi = \pi/2$, the amplitude of the current oscillations is of the order of $(e \sim \hbar) (\hbar \omega)^2$. The oscillation period in the critical current is roughly set by $L = \pi$, similar to the normal-state case of the Datta-Das transistor [5]. Moreover, by systematic variation of the magnetic field (b) direction within the x - y plane, one could measure the SO angle from the Josephson current, see Eq. (21).

B. Two-level dot

In order to get SO-related effects on the Josephson current without a magnetic field, $b = 0$, we study a QD with two levels as a minimal model. As a concrete example, consider the dot states given by the first two oscillator eigenstates ($n_y = 0; 1$) in the longitudinal ground state ($n_x = 1$), such that the energy levels are encoded in $\epsilon_2 - \epsilon_1 = \hbar\omega$ and $\epsilon_0 = (\epsilon_1 + \epsilon_2)/2$. Note that $n_y \notin n_y^0$ is necessary for $A_{nn^0} \neq 0$, see Eq. (10).] Now all matrix elements of B and A are zero except for $A_{12} = A_{21}$, with A_{12} given by

$$A^2 = \frac{\hbar^2 \omega^2}{2m} \sin^2(2\phi) + F_1(L) \cos^2(2\phi) : \quad (24)$$

One easily checks that $\det S = 1$ and therefore the Josephson current now depends on ϕ and L exclusively through Eq. (24).

Figure 3 shows typical numerical results based on Eq. (19) for the critical current I_c as a function of ϕ for two choices of the hybridization parameters n_{nn} , with $\epsilon_{12} = \epsilon_{11} - \epsilon_{22}$. Here we consider a pure Rashba coupling ($\alpha = 0$), and the dot levels are determined by $\epsilon_0 = 0$ and $\hbar\omega = 20$ meV. The shown range for L can be realized in InAs-based devices [11], and thus the supercurrent can be strongly modified by experimentally relevant SO couplings in multi-level quantum dots, with pronounced minima or maxima in I_c . The apparent cusp-like maximum in Fig. 3 is smooth and does not represent singular behavior.

Note that the results displayed in Fig. 3 are for large $\phi = \pi/2$, where the Josephson current is predominantly carried by the Andreev bound state contribution $I_A(\phi)$. The latter can be analytically evaluated from Eqs. (17) and (19) for $(\epsilon_{11} + \epsilon_{22}) = \epsilon_0$, and (at $T = 0$) is expressed in terms of an effective transmission probability T_0 as in Refs. [1, 8],

$$I_A(\phi) = \frac{e}{2\pi} \frac{T_0 \sin \phi}{1 - T_0 \sin^2(\phi/2)} ; \quad (25)$$

where we find $T_0 = 1/(1 + z^2)$ with

$$z = \frac{A^2 + \hbar^2 \omega^2/4}{(\epsilon_{11} + \epsilon_{22}) (\epsilon_0 - \epsilon_2 = 2m) + (\epsilon_{11} - \epsilon_{22}) \hbar\omega/2} : \quad (26)$$

The minimum in I_c is thus expected when $T_0 \rightarrow 0$, in accordance with the values seen in Fig. 3. (For the dashed curve in Fig. 3, the I_c minimum is at $\phi = 0$.) On the other hand, the maximum in I_c (where I_c may exceed the $\phi = 0$ value) is found for $T_0 = 1$, again explaining the numerical result in Fig. 3. Here the level shift $\epsilon_2 = (2m)$ brings one dot level into resonance and thereby causes the enhanced supercurrent. This simple reasoning also explains why the position of the I_c maximum depends only very weakly on the n_{nn} .

The resonance condition, however, depends trigonometrically on the SO coupling via A^2 , see Eq. (24). It results from the interplay between SO couplings and the multilevel nature of the QD. By the description in terms of Andreev bound states, we can also understand why for large dots (long or wide), the effect of the SO coupling is negligible. First, for a 'long' dot, taking $\alpha = 0$, A^2 decreases as L^{-2} , and therefore the SO effects on the Josephson current vanish as $L \rightarrow \infty$. Second, when the lateral dimension of the dot is large, the confinement frequency ω_c becomes small. Now A^2 contains ω_c as a prefactor, and hence is once again suppressed. In both situations, the effect of the SO interaction is merely reduced to a shift of energy levels.

A qualitative argument in favor of such a resonance process can be reached as follows. Schematically, when a Cooper pair enters the dot from the left, either its electrons occupy the same transverse level or they can choose different 'paths' (different transverse levels), in a manner quite similar to a cross-Andreev scattering process [24]. The SO interaction acts differently in these two levels because the longitudinal momenta of both states are not identical. Two electrons entering the QD from, say, the left electrode have initially antiparallel spins, but their respective spins now precess at different rates because of this mismatch in longitudinal momentum. Depending on the value of L , the two electrons which then exit the QD at the right side may, however, be brought back to an antiparallel configuration, leading to a resonance in the critical current caused by the presence of SO couplings. On the other hand, if the spins do not reach the antiparallel configuration, the Josephson current will be reduced.

Note that more than one resonance can be achieved by a careful choice of parameters. This effect is illustrated in Fig. 4. For a multi-level dot with small confinement frequency, the multiple resonances associated with all possible pairs of paths (pairs of levels) will start to overlap significantly. It is then natural to expect that in the limit of very wide quantum dots, these averaging effects will wash out any SO-related structures in the Josephson current, consistent with the results of Ref. [8] for infinite width.

V. CONCLUSION

To conclude, we have studied the Josephson current through a multi-level quantum dot in the presence of Rashba and Dresselhaus spin-orbit couplings. In the absence of electron-electron interactions on the dot, this problem is exactly solvable, a simple consequence of the fact that the Hamiltonian is quadratic in the creation/annihilation operators. (Our model consists of a noninteracting quantum dot including spin- $\uparrow\downarrow$ processes and connected to BCS superconducting leads.) Nevertheless, the combination of superconducting leads and spin- $\uparrow\downarrow$ terms renders a calculation of the Josephson current a quite technical task, which we chose to address via functional integral techniques. We have explicitly shown results for one and two levels, but our general expressions can be applied to arbitrary situations.

For a single dot level, spin-orbit effects cancel out unless a magnetic Zeeman field is included. In this case, we predict spin precession (Datta-Das) effects in the Josephson current, i.e. oscillations as a function of the effective length of the dot. These oscillations have amplitude of the order of a few tenths of the nominal critical current, which should be observable. They result from the interplay between the period of the oscillating effective magnetic field (caused by the combined effects of the Zeeman and Rashba interactions) with the wavelength of the longitudinal modes in the dot.

More interestingly, for the case of a double dot, spin precession effects show up even in the absence of an external magnetic field. This is a novel effect in the field of Josephson physics for devices subject to spin-orbit coupling. The supercurrent can be drastically modified, either containing sharp peaks or being largely suppressed. The experimental observation of such peaks could constitute evidence for spin-orbit effects in a superconducting transistor.

Possible extensions of this work could include Coulomb interaction effects in the dot, which will be important when the tunneling rates become comparable to the dot charging energy. While the inclusion of such effects is beyond the scope of this paper, the present formulation of the problem with functional integral techniques can be adapted to include them in an approximate manner. Nevertheless, we stress again that the high transparency limit considered here is in fact quite relevant in the light of recent experiments where quantum dots are embedded in a Josephson setting using InAs nanowires [17, 18].

Acknowledgments

R.E. and L.D. acknowledge support from the EU network HYSWITCH. T.M. acknowledges support from a CNRS Action Concertée Nanosciences and from an ANR PNANO Grant.

APPENDIX A

In this appendix, we provide some details concerning the derivation of the action in Sec. II. The partition function is here calculated by using the path-integral approach. For this purpose, we rewrite the Hamiltonian in terms of Grassmann-Nambu spinors. We introduce two types of Nambu spinors ('spin-up' and 'spin-down') for the QD fermions,

$$d_n = \begin{pmatrix} d_n^\uparrow \\ d_n^\downarrow \end{pmatrix}; \quad d_n^c = \begin{pmatrix} d_n^\uparrow \\ d_n^\downarrow \end{pmatrix}^T;$$

while the BCS leads are described by the conventional 'spin-up' Nambu spinor, $\psi_{jk} = (\psi_{jk}^\uparrow; \psi_{jk}^\downarrow)^T$. With the notation introduced in Sec. II, we can then effectively write

$$H_D = \sum_n d_n^\dagger \left(\frac{t_n^2}{2m} \right) d_n + A_{z,nm} d_n^\dagger + B_{z,nm} d_n^\dagger d_m + \sum_{nm} \frac{1}{2} d_n^\dagger (A_{+,nm} + B_{-,nm} d_n^c) d_m^c + d_n^c (A_{+,nm} + B_{-,nm} d_n) d_m :.$$

In spinor notation, the tunneling Hamiltonian reads

$$H_T = \sum_{j=L,R} \sum_{kn} \psi_{jk}^\dagger (T_{jn} d_n + T_{jn}^c d_n^c) + h.c. :$$

After gauging out the phase from the leads,

$$T_{j=L=R,n} = \cos(L/2) e^{i\phi_n} \begin{pmatrix} t_{jn} & 0 \\ 0 & t_{jn} \end{pmatrix};$$

$$T_{j,n} = \sin(L/2) e^{i\phi_n} e^{i\phi_n} \begin{pmatrix} t_{jn} & 0 \\ 0 & t_{jn} \end{pmatrix} :$$

After integrating out the ψ_{jk} and taking into account the relation between the Fourier transformed 'spin-up' and 'spin-down' Nambu spinors for the QD, see Eq. (14),

$$D_n(!) = \frac{1}{T} \int_0^T d\tau e^{i\tau} d_n(\tau); \quad \psi_n D_n(!) = \frac{1}{T} \int_0^T d\tau e^{i\tau} d_n^c(\tau);$$

we obtain the effective action

$$S = S_D - \sum_{!nm} \sum_j D_n(!) D_n(!) \sum_j \begin{pmatrix} T_{jn}^y g! T_{jm} & T_{jn}^y g! T_{jm}^x \\ x T_{jn}^y g! T_{jm} & x T_{jn}^y g! T_{jm}^x \end{pmatrix} \begin{pmatrix} D_m(!) \\ D_m(!) \end{pmatrix}; \quad (A1)$$

where $g!$ denotes the Green's function of the uncoupled leads

$$g! = \frac{1}{i\omega_n + \frac{\epsilon_n}{2}} (i\omega_n + \frac{\epsilon_n}{2}) :$$

Notice that there is no contribution from the gauged-out spin- $\frac{1}{2}$ terms describing spin precession along the transport direction, since in the second term of Eq. (A1), all odd terms vanish. Finally, the action of the closed QD is

$$S_D = \sum_{!nm} \sum_j D_n(!) \left(i\omega_n + \frac{\epsilon_n}{2} \right) d_n + A_{z,nm} d_n + B_{z,nm} d_n d_m + \frac{1}{2} D_n(!) (A_{+,nm} d_n + iB_{-,nm} d_n^c) d_m + D_n(!) (A_{+,nm} d_n + iB_{-,nm} d_n^c) d_m :.$$

To simplify calculations, we now assume $t_{jn} = t_{jn}$. Introducing the multispinor (15), after some algebra, we then find the effective action (16) with Eq. (17), where $\hat{G}!$ is the full Green's function of the QD for $\epsilon = 0$ (except for the shift in energy),

$$\hat{G}_{!,nn^0}^{-1} = i\omega_n + \frac{\epsilon_n}{2} = (2m) \left(\frac{\epsilon_n}{2} + \frac{(\epsilon_L + \epsilon_R)_{nn^0}}{2} \right) \left[i\omega_n + \cos(L/2) \right] + \frac{(\epsilon_L - \epsilon_R)_{nn^0}}{2} \sin(L/2) \gamma \quad (A2)$$

with the hybridization matrix given by Eq.(18).

-
- [1] A.A. Golubov, M.Yu. Kupriyanov, and E. Il'ichev, *Rev. Mod. Phys.* **76**, 411 (2004).
 - [2] Yu.A. Bychkov and E.I. Rashba, *J. Phys. C* **17**, 6039 (1984).
 - [3] S.W. Eiss and R. Egger, *Phys. Rev. B* **72**, 245301 (2005).
 - [4] J.M. Elzerman, R. Hanson, L.H. Willems van Beveren, B.W. Itkamp, L.M.K. Vandersypen, and L.P. Kouwenhoven, *Nature* **430**, 431 (2004).
 - [5] S. Datta and B. Das, *Appl. Phys. Lett.* **56**, 665 (1990).
 - [6] E.V. Bezuglyi, A.S. Rozhavsky, I.D. Vagner, and P. Wyder, *Phys. Rev. B* **66**, 052508 (2002).
 - [7] I.V. Krive, A.M. Kadigrobov, R.I. Shekhter, and M. Jonson, *Phys. Rev. B* **71**, 214516 (2005).
 - [8] O.V. Diniltrova and M.V. Feigel'man, *J. Exp. Theor. Phys.* **102**, 652 (2006).
 - [9] A. Furusaki and M. Tsukada, *Physica B* **165**, 967 (1990).
 - [10] C.W.J. Beenakker and H. van Houten, *Phys. Rev. Lett.* **66**, 3056 (1991).
 - [11] J.Nitta, T. Akazaki, H. Takayanagi, and T. Enoki, *Phys. Rev. Lett.* **78**, 1335 (1997); G. Engels, J. Lange, T. Schapers, and H. Luth, *Phys. Rev. B* **55**, R1958 (1997).
 - [12] H. Takayanagi, T. Akazaki, and J. Nitta, *Phys. Rev. Lett.* **75**, 3533 (1995).
 - [13] Th. Schapers, V.A. Guzenko, R.P. Muller, A.A. Golubov, A. Brinkman, G. Creelius, A. Kaluza, and H. Luth, *Phys. Rev. B* **67**, 014522 (2003).
 - [14] F. Giazotto, K. Grove-Rasmussen, R. Fazio, F. Beltram, E.H. Lindeld, and D.A. Ritchie, *J. Supercond.* **17**, 317 (2004).
 - [15] M. Ebel, C. Busch, U. Merkt, M. Gajar, T. Plecenik, and E. Il'ichev, *Phys. Rev. B* **71**, 052506 (2005).
 - [16] J.-P. Cleuziou, W. Wemsdorfer, V. Bouchiat, T. Ondarcuhu, and M. Monthieux, *Nature Nanotechnology* **1**, 53 (2006).
 - [17] Y.J. Doh, J.A. van Dam, A.L. Roest, E.P.A.M. Bakkers, L.P. Kouwenhoven, and S. De Franceschi, *Science* **309**, 272 (2005).
 - [18] J.A. van Dam, Yu.V. Nazarov, E.P.A.M. Bakkers, S. De Franceschi, and L.P. Kouwenhoven, *Nature* **442**, 667 (2006).
 - [19] K. Flensberg, *Phys. Rev. B* **48**, 11156 (1993); K.A. Matveev, *Phys. Rev. B* **51**, 1743 (1995); Yu.V. Nazarov, *Phys. Rev. Lett.* **82**, 1245 (1999).
 - [20] Q.F. Sun, J. Wang, and H. Guo, *Phys. Rev. B* **71**, 165310 (2005).
 - [21] A. Levchenko, A. Kamenev, and L.I. Glazman, *cond-mat/0601177*.
 - [22] N.M. Chtchelkatchev and Yu.V. Nazarov, *Phys. Rev. Lett.* **90**, 226806 (2003).
 - [23] E. Vecino, A. Martn-Rodero, and A. Levy Yeyati, *Phys. Rev. B* **68**, 035105 (2003). See also: C. Benjamin, T. Jonckheere, A. Zazunov, and T. Martin, *cond-mat/0605338*.
 - [24] J. Torres and T. Martin, *Eur. Phys. J. B* **12**, 319 (1999); G. Deutscher and D. Feinberg, *Appl. Phys. Lett.* **76**, 487 (2000).

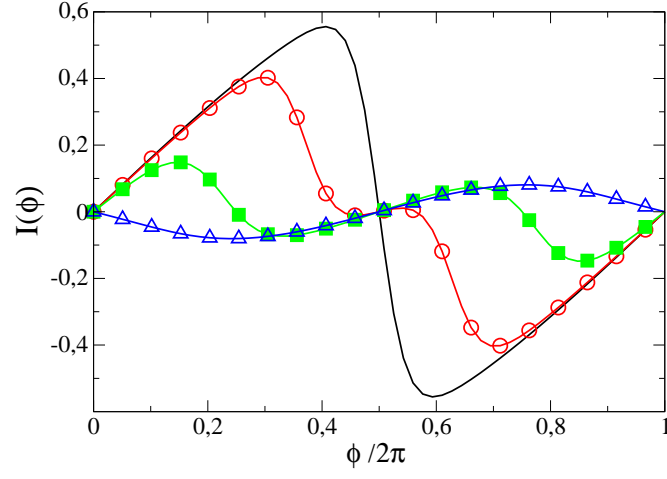


FIG .1: (Color online) Josephson current in units of $e\hbar$ through a single-level QD with $\mu = 0$; $T = 0$; $\Gamma = 2$ for $B = 0$ (solid curve), 0.4 (circles), 0.8 (squares), and 1.2 (triangles).

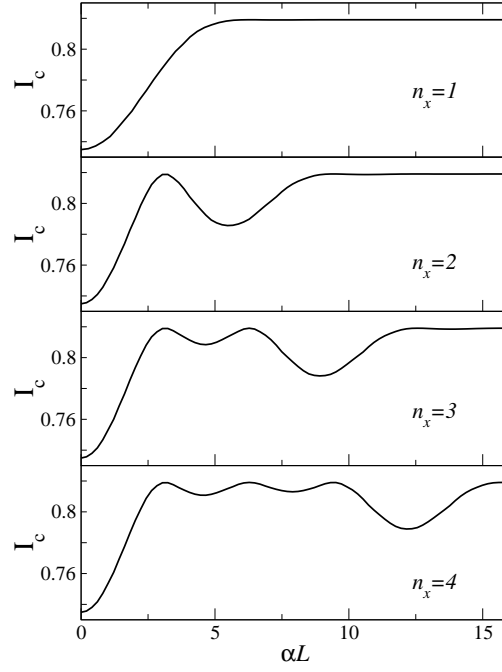


FIG .2: SO-induced oscillations of the critical current I_c (in units of $e\hbar$) in a single-level dot as a function of L for $b = (0; 0; 0.2)^T$; $\mu = 10$; $T = 0.05$. The dot is taken in the transverse ground state $n_y = 0$, with only one resonant level $n_x = 0$, for various n_x .

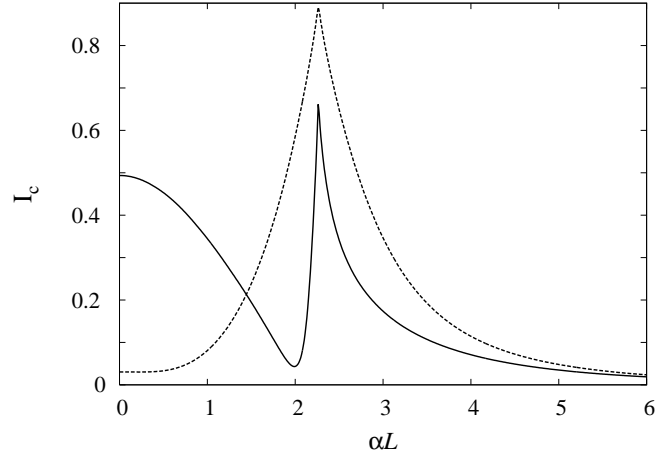


FIG. 3: Zero-field critical current as a function of αL in a two-level quantum dot. We take $\epsilon_0 = 0$, $\epsilon_2 = 20$ meV, $\epsilon_1 = 0$, $\epsilon_3 = 1$ meV, $L = 20$ nm, $m = 0.035m_e$, and $T = 0.01$. (These values are appropriate for Nb contacts.) Results are shown for two cases (where $\epsilon_{12} = \sqrt{\epsilon_{11}\epsilon_{22}}$), namely either $\epsilon_{11} = 20$ and $\epsilon_{22} = 0$ (only one level couples to the leads, solid line) or $\epsilon_{22} = \epsilon_{11} = 10$ ('democratic tunneling', dashed line).

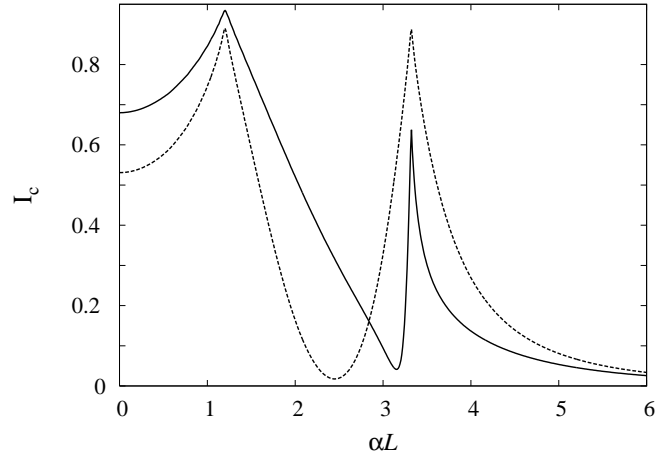


FIG. 4: Same as Fig. 3, but for $\epsilon_0 = 15$ meV.